Journal Pre-proofs

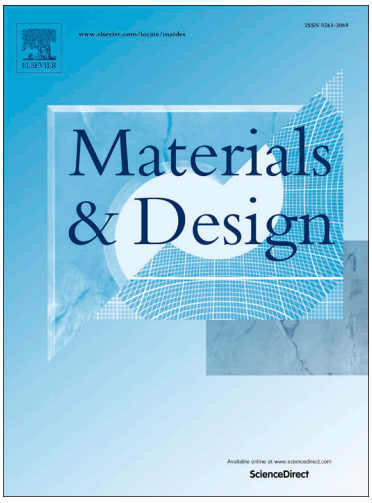

Development of pH-responsive and antibacterial semi-IPN hydrogel films based on carboxymethylcellulose and tetraethyl orthosilicate

Gelare Sadeghi Borojeni, Majid Kolahdoozan, Rokhsareh Meamar

PII: S0264-1275(26)01292-X
DOI: https://doi.org/10.1016/j.matdes.2026.116717
Reference: JMADE 116717

To appear in: *Materials & Design*

Received Date: 11 February 2026
Revised Date: 14 July 2026
Accepted Date: 30 July 2026

Please cite this article as: Borojeni, G.S., Kolahdoozan, M., Meamar, R., Development of pH-responsive and antibacterial semi-IPN hydrogel films based on carboxymethylcellulose and tetraethyl orthosilicate, *Materials & Design* (2026), doi: https://doi.org/10.1016/j.matdes.2026.116717

Development of pH-Responsive and Antibacterial Semi-IPN Hydrogel Films Based on Carboxymethylcellulose and Tetraethyl Orthosilicate

Gelare Sadeghi Borojeni[1], Majid Kolahdoozan*[2], Rokhsareh Meamar[3]

[1] Department of Chemistry, Shah. C., Islamic Azad University, Shahreza, P.O. Box 311-86145, Islamic Republic of Iran
[2] Department of Chemistry, Institute of Agriculture, Water, Food, and Nutraceuticals, Isf. C., Islamic Azad University, Isfahan, Islamic Republic of Iran
[3] Isfahan Clinical Toxicology Research Center, Isfahan University of Medical Sciences, Isfahan, Iran

Abstract

Multifunctional hydrogel films which could combine pH responsiveness, antibacterial activity, and cytocompatibility are attractive for advanced biomedical and functional applications. In this study, semi-interpenetrating polymer network (semi-IPN) hydrogel films were fabricated from sodium carboxymethyl cellulose (CMC) and tetraethyl orthosilicate (TEOS), followed by the incorporation of silver chloride (AgCl) to introduce antibacterial functionality. The structure, morphology, and thermal properties of the films were investigated using X-ray diffraction (XRD), Fourier-transform infrared spectroscopy (FT-IR), scanning electron microscopy (SEM), thermogravimetric analysis (TGA), and differential scanning calorimetry (DSC). The developed hydrogels exhibited reversible pH-dependent swelling, reaching approximately 850 ± 34% in alkaline media while shrinking under acidic conditions. Ag-containing films inhibited the growth of both Escherichia coli and Bacillus subtilis, producing inhibition zones of 9.5 mm for each strain. Cytocompatibility evaluation using the MTT assay demonstrated excellent fibroblast viability after 7 days, with cell viabilities of 97.49 ± 0.85% for CMC films and 93.68 ± 2.40% for Ag-containing films, satisfying ISO 10993-5 requirements. The combination of simple processing, inexpensive raw materials, pH-responsive behavior, antibacterial performance, and cytocompatibility highlights the potential of these semi-IPN hydrogel films for applications including wound dressing, controlled drug delivery, active food packaging, biosensing, and agricultural technologies.

Keywords: Carboxymethylcellulose, SiO_2, Semi-IPN Films, Smart hydrogel, Silver chloride

* Corresponding Author:

E-mail: kolahdoozan@iau.ac.ir, mkolahdoozan@gmail.com (M. Kolahdoozan)

1. Introduction

Hydrogels have attracted considerable attention as soft polymeric biomaterials for biomedical and pharmaceutical applications because of their ability to absorb and retain large amounts of water while maintaining their three-dimensional cross-linked network structure [1]. Their swelling behavior, which largely determines their functional performance, depends on several factors including polymer composition, network architecture, crosslinking density, and the characteristics of the surrounding medium [1]. Among hydrogel-forming materials, naturally derived polysaccharides such as starch [2,3], sodium carboxymethyl cellulose (CMC) [4–6], chitosan [7–9], alginate [10], and cellulose [11] are particularly attractive because of their biodegradability, biocompatibility, and excellent water-retention capability. These characteristics make polysaccharide-based hydrogels attractive candidates for a broad range of biomedical applications, including drug delivery and tissue engineering [6,8,12].

An effective strategy to overcome the intrinsic mechanical limitations of natural polymer hydrogels is the construction of interpenetrating polymer networks (IPNs), which enhance structural stability, elasticity, and swelling performance while preserving the favorable characteristics of the parent polymers [1]. IPNs consist of two or more polymer networks that are physically interlaced without covalent bonds between them, resulting in materials with superior physicochemical properties compared with conventional single-network hydrogels [13,14]. Depending on their architecture, IPNs are generally classified as full-IPNs and semi-IPNs [15]. In full-IPNs, both polymer components are crosslinked simultaneously to form interpenetrating networks, whereas semi-IPNs consist of one crosslinked polymer network physically penetrated by a second linear or branched polymer without additional crosslinking [16]. Owing to their structural versatility, IPNs have evolved from conventional engineering

materials into multifunctional biomaterials for a wide range of biomedical applications [16–18]. By tailoring polymer composition, IPNs can be engineered to respond to external stimuli such as pH, temperature, light, magnetic fields, ionic strength, redox conditions, mechanical stress, and enzymatic activity [19,20]. Consequently, IPN hydrogels have been widely explored for tissue engineering, regenerative medicine, drug delivery, chemical processing, and smart sensing applications [5,6,21–24]. Among these applications, drug delivery has attracted particular attention because IPN hydrogels enable controlled release of therapeutic agents while minimizing systemic toxicity and reducing adverse effects [25,26]. In particular, pH-responsive IPN hydrogels have attracted considerable interest owing to their ability to achieve site-specific drug release in physiological environments with distinct pH values, including gastric fluid, tumor microenvironments, and the colon [3,8,27–29].

CMC a water-soluble cellulose derivative, has been extensively investigated as a hydrogel matrix because of its excellent biocompatibility, pH responsiveness, high water absorption capacity, and low cost, making it an attractive candidate for scalable biomedical and pharmaceutical applications [4,5]. Nevertheless, the poor mechanical strength and limited film-forming ability of CMC-based hydrogels restrict their practical use and often require structural reinforcement [6]. Tetraethyl orthosilicate (TEOS), a widely used silica precursor, offers an effective strategy for improving these limitations. Through hydrolysis and condensation reactions, TEOS generates inorganic silica networks that enhance the mechanical stability and structural integrity of organic–inorganic hybrid materials [30,31]. Incorporating silica into CMC-based hydrogels therefore provides an opportunity to develop robust hybrid networks with improved physicochemical performance [32]. Despite these advances, the development of flexible pH-responsive CMC/SiO_2 semi-IPN hydrogel films suitable for coating and biomedical applications remains insufficiently explored. More importantly, the structural

interactions governing the formation of the semi-IPN architecture and their influence on swelling behavior and biological performance have not yet been systematically clarified.

In this study, we hypothesized that hydrogen-bond-mediated physical interpenetration between CMC chains and the TEOS-derived silica network would generate flexible semi-interpenetrating polymer network (semi-IPN) hydrogel films with enhanced structural integrity and pH-responsive swelling behavior. Furthermore, the incorporation of silver ions into the hybrid network was expected to improve antibacterial activity without compromising the physicochemical performance of the films. To validate this hypothesis, flexible CMC/SiO_2 semi-IPN hydrogel films were fabricated through a simple and environmentally friendly approach. The resulting films were systematically characterized in terms of their network structure, pH-responsive swelling behavior, cytocompatibility, and antibacterial activity. This study provides new insights into the structure–property relationship of CMC/SiO_2 semi-IPN hydrogel films and expands their potential for pH-responsive biomedical coatings and controlled drug-delivery applications.

2. Materials and Methods

2.1. Materials

Tetraethyl orthosilicate ≥99.5% (TEOS), hydrochloric acid (fuming, 37%), and silver nitrate 99% ($AgNO_3$) were purchased from Merck KGaA, Germany. Sodium carboxymethyl cellulose (CMC) 99.5% was provided by CP Kelco, Norway (Cekol 4000, DS: 0.8, Mw: 450 kDa, DP: 2000, source: wood pulp). Ethanol (EtOH, 96%; Razi Yeast and Alcohol Co., Iran) and distilled water were used as starting materials. All chemicals were used as received without further purification.

2.2. Preparation of CMC/SiO_2 semi-IPN film

To prepare the silica precursor solution, 1.04g of TEOS and 7.5 mL of ethyl alcohol were stirred at 25°C in a 250 mL Erlenmeyer flask. A blend of ethanol (5 mL) and distilled water (12.5 mL) containing 0.045 wt% HCl was gradually added to the solution under continuous stirring. This mixture was stirred for 24 hours at 25°C to allow hydrolysis and condensation reactions to occur. Concurrently, a CMC solution was prepared by dissolving 1.04 g of CMC in 32.5 g of water and stirring for 6 h at 25 C.

The prepared CMC solution was then added to the hydrolyzed TEOS network under vigorous stirring. After 24 h of stirring, a homogeneous solution was obtained. This solution was poured into a large Pyrex crystallizing dish and kept at 25 C to cast the film.

To evaluate and optimize the effect of different components, the same procedure was repeated using varying amounts of TEOS (0.52, 1.04, and 1.56 g) and CMC (0.52 and 1.04 g) to yield TEOS/CMC weight ratios of 1:1, 2:1, 3:1, and 1:2.

2.3. Loading of Ag compound

Silver ion was incorporated into the IPN structures as a potent antiseptic agent. Silver nitrate was added to the TEOS solution during the hydrolysis and condensation steps. Different amounts of $AgNO_3$ were used to produce hybrids with silver ion contents of 0.1 wt%, 0.3 wt%, and 0.5 wt%. Each TEOS/ $AgNO_3$ mixture was sonicated three times for 10 minutes using a Power Sonic 405 ultrasonic bath (manufactured in Korea by Hwashin Technology Co.) at 25°C to disperse the particles. After dispersion, the mixture was added to the CMC solution, following the same procedure described in Section 2.2. Adding the TEOS/AgCl precursor solution dropwise into the stirring viscous CMC solution ensures a more uniform distribution of AgCl particles and hydrolyzed silica species throughout the polymer matrix, minimizing particle agglomeration and localized silica-rich regions formed by premature condensation. The final result was the CMC/SiO_2/AgCl semi-IPN film.

2.4. Characterizations

To investigate the crystallinity of the IPN hybrid, X-ray diffraction data were obtained using an X'Pert Pro PMD diffractometer in the 2θ range of 10–80°. Morphological analysis of the films was performed using scanning electron microscopy (SEM). The smooth surfaces and free of burrs sample was chosen and then carefully was fixed on the stop using carbon glue. After fixing the sample, it was transferred to a gold coater and the surface of the sample was coated with gold using a sputtering process. After gold plating, the sample was transferred to the FESEM chamber and set for testing. The internal morphology was examined using a TESCAN Mira III field emission SEM (FESEM), manufactured in the Czech Republic. The IPN structural building units were studied by FT-IR spectroscopy using a Perkin-Elmer Fourier Transform Infrared (FTIR) spectrometer (Model 1750, manufactured in the United States) with a resolution of 2 cm^{-1}, operating in the spectral range of 4000–500 cm^{-1}. Neat films were mounted in a magnetic sample holder and directly positioned in the sample compartment. Thermogravimetric (TG) analysis of thin CMC/SiO_2 and CMC/SiO_2/AgCl films was performed to evaluate the effect of interpenetration between CMC, SiO_2, and AgCl on the thermal degradation and stability of the hybrid films. A Q600 thermal analyzer (TA Instruments, United States) was used under a nitrogen (N_2) atmosphere, with a heating rate of 20 °C/min, to obtain TG, TGA, and DSC data.

2.5. Swelling and dynamic swelling properties

The swelling and dynamic swelling ratio of the semi-IPN film was evaluated in phosphate-buffered saline (PBS) solutions at pH 3 and 10, using the gravimetric technique [33]. Dried samples of known weight were immersed in the PBS solutions for 24 hours at 25°C. At specific time intervals (to 24 h), samples were removed, surface moisture was gently blotted with tissue paper (avoiding excessive pressure), weighed, and then re-immersed in the aqueous medium. The swelling ratio was calculated using the following expression:

$$S_{wt} = \frac{w_t - w_0}{w_0} \times 100 \qquad (1)$$

where w_0 is the weight of the dried initial sample, and w_t is the weight of the swollen sample at time t. To estimate the dynamic swelling performance, one dried sample was first immersed in PBS solution at pH 3 for 5 minutes. After weighing, the same sample was then immersed in PBS solution at pH 10 for another 5 minutes, and this cycle was repeated for a total duration of 60 minutes [34].

2.6. Antibacterial activity studies by Agar disk-diffusion method

Both gram-positive *Bacillus subtilis* and gram-negative *Escherichia coli* were used to evaluate the antibacterial effect of thin CMC/SiO_2 and CMC/SiO_2/AgCl semi-IPN films. The strains were obtained from the Food Science Laboratory of Islamic Azad University and were cultured on LB agar plates for 18 hours at 37 °C prior to use. A suspension of the isolates (approximately 1–2 × 10^8 CFU/mL) was prepared according to the McFarland standard, and spread evenly onto Müller-Hinton agar in Petri dishes. Then, semi-IPN filter discs (approximately 7 mm in diameter) were placed on the agar surface. The Petri dishes were incubated for 24 hours, and the diameters of the inhibition zones around each disc were measured using a caliper to assess the antimicrobial effect.

2.7. MTT ASSAY

Fibroblast cell lines obtained from the Pasteur Institute were used to assess the metabolic activity and cytotoxicity of the produced films. This part of the research was conducted under the ethical approval code IR.IAU.DEHAGHAN.REC.1398.005.

3. Results and Discussion

3.1. Influence of precursor composition on semi-IPN film formation

The composition of the precursor solution played a critical role in determining the physical integrity and processability of the semi-IPN hydrogel films [35–37]. Therefore, different mass ratios of CMC, TEOS, HCl, and $AgNO_3$ were systematically optimized based on previous

studies and preliminary experiments to obtain flexible, mechanically stable, and nearly transparent thin films (thickness of ~0.3 mm) suitable for wound-dressing applications (Fig. 1) [38].

Increasing the TEOS content markedly improved film rigidity but simultaneously reduced flexibility and structural integrity. This behavior can be attributed to the formation of a denser SiO_2 network, which restricts polymer-chain mobility and limits structural deformation. Consequently, films prepared with excessive TEOS exhibited characteristics dominated by the inorganic silica framework rather than by a balanced organic–inorganic semi-IPN structure. Similar trends have been reported previously [32,39–41].

CMC acted as the pH-responsive polymeric phase of the semi-IPN films [4,42,43]. As the amount of CMC increased, the film thickness also increased, while mechanical strength decreased. The increased porosity facilitated water uptake and improved swelling behavior; however, it also weakened the structural integrity of the films.

With higher CMC content, the films exhibited more pores, resulting from CMC aggregation, which prevented uniform coverage of the SiO_2 network. While these pores contributed to improved swelling behavior, they also increased film permeability and thickness, resulting in reduced structural cohesion. Accordingly, the 1:1 CMC/TEOS ratio provided the best compromise between flexibility, structural integrity, and swelling performance, and was therefore selected for subsequent experiments.

The incorporation of $AgNO_3$ altered the physical characteristics of the semi-IPN films. Among the investigated formulations, 0.3 wt% $AgNO_3$ provided the best balance between film integrity and antibacterial functionality. However, increasing the silver content reduced film flexibility and swelling capacity. This behavior was attributed to the formation of larger Ag-containing domains and particle aggregation, which increased local rigidity and disrupted the continuity of the polymeric network. At higher $AgNO_3$ concentrations, film fragmentation and loss of

structural uniformity were observed. The influence of silver incorporation on the chemical structure and intermolecular interactions is discussed in the following section.

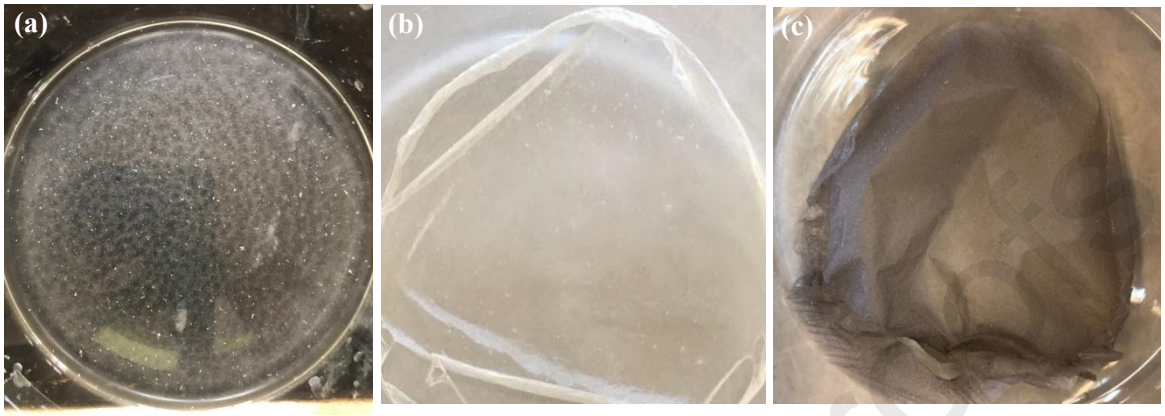

Figure 1. Visual comparison of semi-IPN films: (a) CMC/SiO_2 before drying, (b) CMC/SiO_2 after drying, (c) CMC/SiO_2/AgCl after drying.

3.2. Characterizations

Figure 2 shows the XRD patterns of neat CMC, the SiO_2 network, CMC/SiO_2 semi-IPN, and CMC/SiO_2/AgCl semi-IPN films. Neat CMC exhibits a broad diffraction halo centered at approximately $2\theta = 20°$, characteristic of its predominantly amorphous structure [44,45]. The SiO_2 network displays a broad halo centered at approximately 23° (JCPDS No. 00-001-0649), confirming its amorphous nature [46]. Four weak diffraction peaks located at 31.9°, 45.8°, 56.9°, and 76.0° were assigned to residual NaCl, corresponding to the (200), (220), (222), and (420) planes of cubic NaCl (JCPDS No. 96-900-6370). Compared with neat CMC, the characteristic diffraction halo became broader and merged with the amorphous silica halo, indicating disruption of the semi-crystalline CMC domains through strong intermolecular interactions with the silica network, resulting in a predominantly amorphous semi-IPN structure. In contrast, the CMC/SiO_2/AgCl semi-IPN film exhibited sharp diffraction peaks at 31.7°, 45.5°, 56.6°, 75.5°, and 84.2° corresponding to the (200), (220), (222), (420), and (422)

reflections of cubic silver chloride (AgCl, JCPDS No. 01-077-2067), confirming the successful in situ formation of AgCl within the CMC/SiO_2/AgCl semi-IPN film [47,48]. In the CMC/SiO2/AgCl composite film, alongside the sharp crystalline peaks of AgCl, a broad halo centered at approximately 23° remained visible. This broad halo is characteristic of the amorphous silica (SiO2) network [49]. The coexistence of the amorphous silica halo and crystalline AgCl reflections indicates successful incorporation of AgCl into the semi-IPN while preserving the amorphous nature of the CMC/SiO_2 matrix.

Figure 3 presents the SEM micrographs of CMC/SiO_2 and CMC/SiO_2/AgCl semi-IPN films. Distinct morphological differences were observed between the CMC/SiO_2 and CMC/SiO_2/AgCl semi-IPN films. The CMC/SiO_2 semi-IPN film exhibited a relatively homogeneous surface with uniformly distributed domains (Figs. 3a–c). Such a morphology has been reported to promote swelling and flexibility, although excessive porosity may compromise mechanical strength [50].

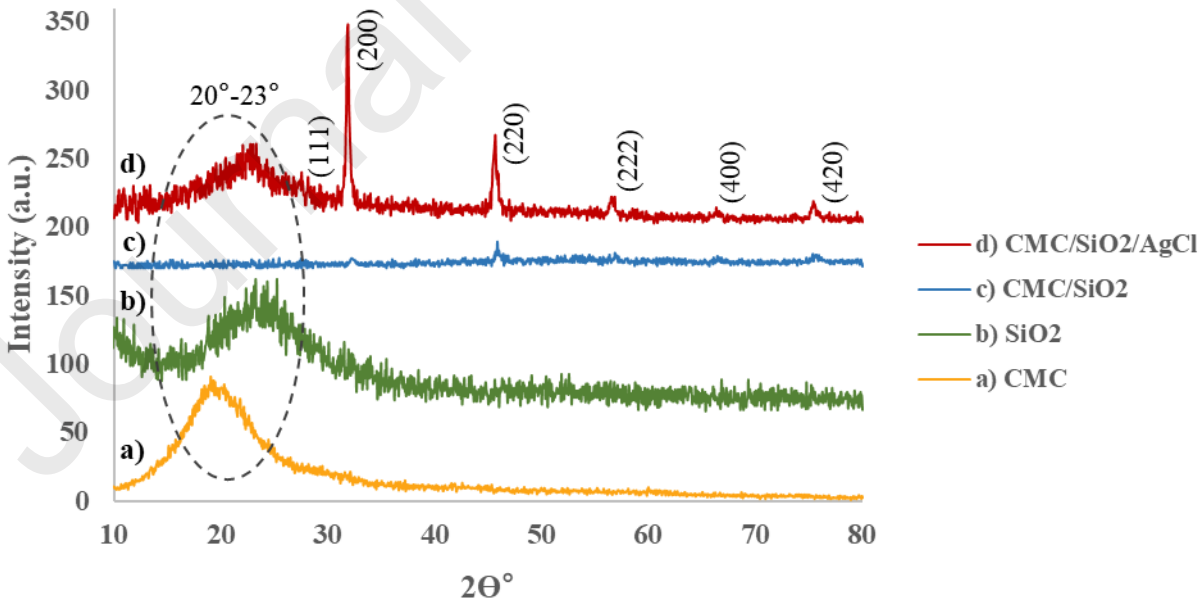

Figure 2. XRD patterns of neat CMC, SiO_2, CMC/SiO_2 and CMC/SiO_2/AgCl semi-IPN films

After $AgNO_3$ incorporation, noticeable changes in surface morphology were observed, including a rougher surface and the appearance of larger surface aggregates (Figs. 3d–f). The appearance of these larger surface aggregates is consistent with the crystalline AgCl phase identified by XRD. These morphological changes may contribute to the reduced swelling behavior observed for the CMC/SiO_2/AgCl semi-IPN. In both groups of semi-IPN films, nanoscale surface features with characteristic dimensions below approximately 30 nm were observed in several regions of the films, consistent with findings reported in previous studies [51,52]. A limitation of the present study is the absence of cross-sectional SEM analysis, as preparation of representative cross-sections frequently caused deformation and damage to the soft hydrogel films. Future work will focus on developing suitable sample-preparation methods for reliable cross-sectional characterization.

Figure 4 presents the FT-IR spectra of CMC, TEOS, CMC/SiO_2, and CMC/SiO_2/AgCl semi-IPN films. The CMC spectrum shows a broad O–H stretching band centered at 3390 cm^{-1} together with the asymmetric CH_2 stretching vibration at 2915 cm^{-1}. Sharp peaks at 1611 cm^{-1} and 1403 cm^{-1} are attributed to the symmetric and asymmetric stretching of carboxylate groups, while a strong band at 1065 cm^{-1} corresponds to the C–O–C stretching vibration [53,54].

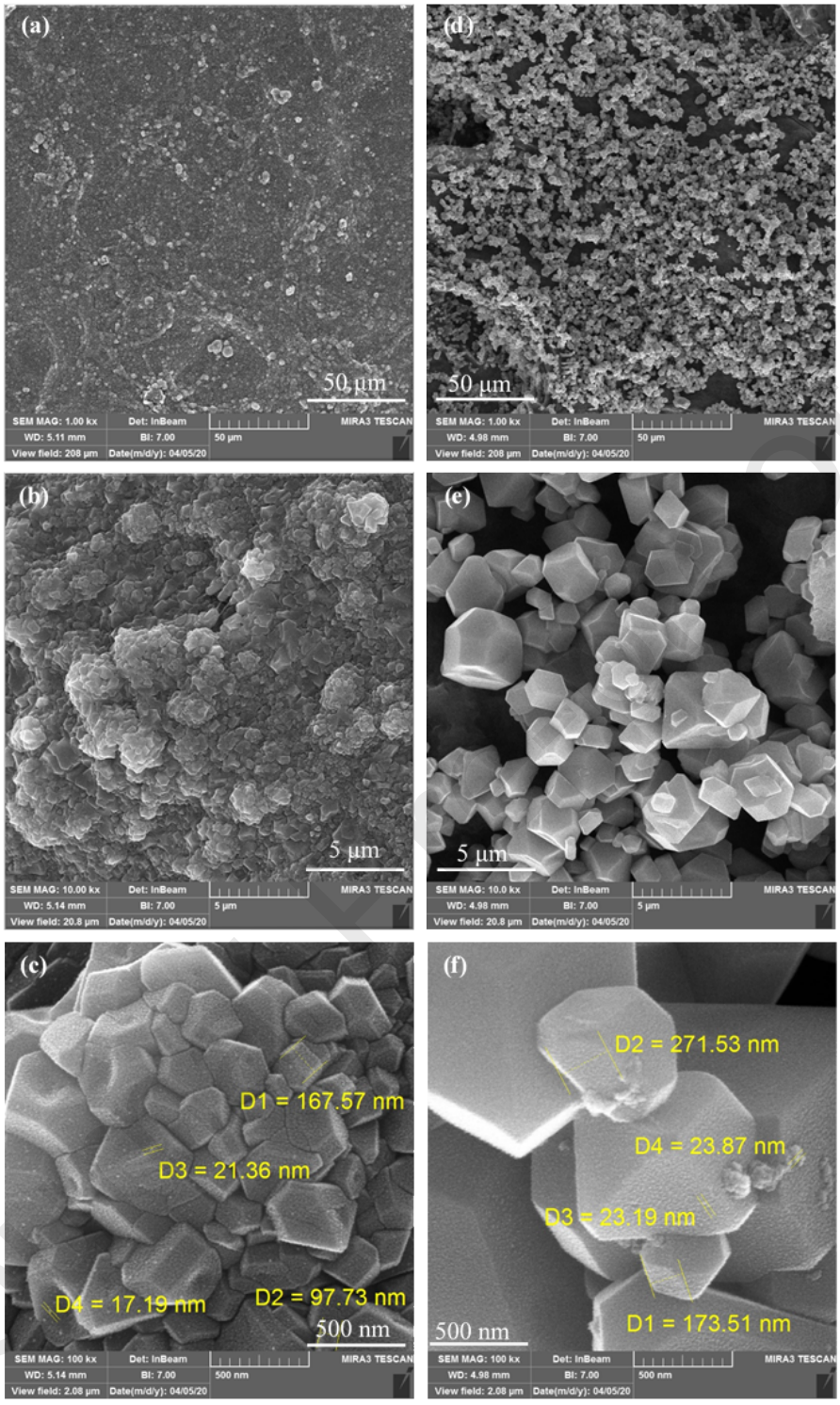

Figure 3. SEM images of CMC/SiO_2 (a, b and c) and CMC/SiO_2/AgCl (d, e and f) semi-IPN films at magnifications of 50 µm, 5 µm and 500 nm.

The FT-IR spectrum of TEOS displays asymmetric stretching peaks of CH_3 and CH_2 at 2981 cm^{-1} and 2931 cm^{-1}, respectively. Bending vibrations of CH_2 and CH_3 appear at

1446 cm^{-1} and 1393 cm^{-1}, while peaks at 1109, 965, 797, and 478 cm^{-1} are assigned to Si–O–Si and Si–O vibrational modes [55–57].

In the CMC/SiO_2 spectrum, the absence of CH_3 stretching and bending peaks at 2981 cm^{-1} and 1393 cm^{-1} confirms the hydrolysis of TEOS and the removal of ethoxy groups during silica network formation. A slight shift from 3390 cm^{-1} in neat CMC to 3373 cm^{-1} in CMC/SiO_2 films suggests hydrogen-bond formation between the hydroxyl groups of CMC and silanol groups within the silica network. In the CMC/SiO_2/AgCl sample, AgCl incorporation does not introduce new characteristic absorption bands; however, slight broadening of the O–H and C–O–C absorption bands suggests enhanced intermolecular interactions within the hybrid network [58,59].

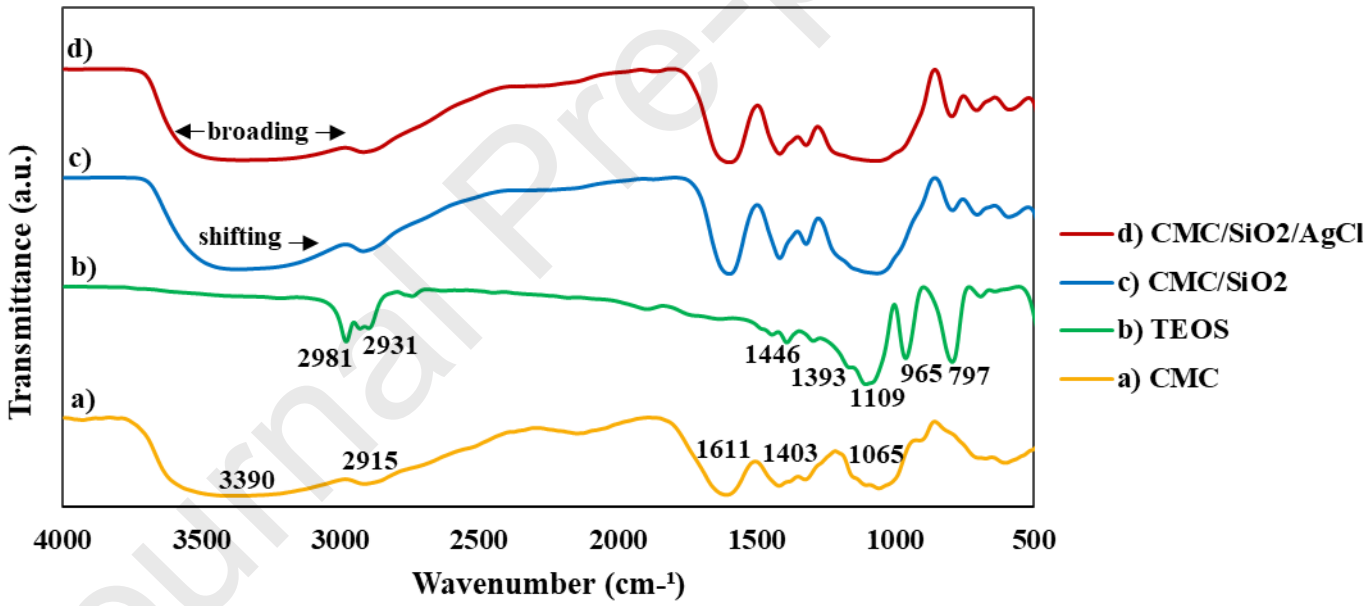

Figure 4. FT-IR spectra of CMC, TEOS, CMC/SiO_2, and CMC/SiO_2/AgCl semi-IPN films

Figure 5 presents the thermal analysis results of the CMC/SiO_2 and CMC/SiO_2/AgCl semi-IPN films, as determined by TGA and DSC analyses. As shown by the thermogravimetric analysis (TGA) curves in Figure 5a–b, three distinct weight-loss stages were observed during heating for both semi-IPN films. The first, minor weight-loss step appears at approximately 115 °C for the CMC/SiO_2 semi-IPN and 111 °C for the CMC/SiO_2/AgCl semi-IPN, and is attributed to the

evaporation of absorbed and physically adsorbed moisture. The second, more pronounced step occurs around 309°C for CMC/SiO_2 and 313°C for CMC/SiO_2/AgCl, corresponding to depolymerization and thermal decomposition of the CMC network. This stage includes the release of CO_2 due to decarboxylation of carboxylic groups in CMC, which accounts for the major weight loss in both samples [60,61].

According to previous reports, pristine CMC typically exhibits an initial weight-loss stage below 150 °C due to the evaporation of absorbed moisture, followed by a major degradation stage within the range of 250–350 °C associated with depolymerization and decarboxylation reactions. The thermal behavior observed for the present semi-IPN films is generally consistent with these literature reports, indicating that the characteristic degradation behavior of CMC is largely preserved after semi-IPN formation, although the incorporation of silica and Ag/AgCl modifies the thermal degradation profile [54,61–63].

As shown in Figure 5c, a distinct exothermic peak appears at the initial stage, indicating an exothermic transition of the CMC/SiO_2 semi-IPN framework. A broad endothermic event between 79 °C and 235 °C corresponds to the vaporization of water trapped within the internal layers of the silica network, as well as the melting of CMC in the hydrogel [64]. Around 330 °C, another broad endothermic peak marks the thermal decomposition of the CMC component within the network. Figure 5d displays the DSC thermogram of the CMC/SiO_2/AgCl semi-IPN sample, which similarly begins with an initial exothermic peak, followed by two endothermic peaks centered near 160 °C and 300 °C, corresponding to water loss and CMC decomposition, respectively. Compared with the CMC/SiO_2 semi-IPN film, the Ag-containing sample exhibits a lower decomposition temperature in the DSC analysis and a reduced decomposition enthalpy (ΔH), which decreases from 102.9 J/g to 52.9 J/g. Although the main degradation step observed in the TGA curves shifts

slightly toward a higher temperature (313 °C versus 309 °C), the DSC results indicate that less energy is required for thermal decomposition after incorporation of Ag/AgCl. These findings suggest that Ag/AgCl incorporation modifies the intermolecular interactions between CMC chains

and the silica framework, thereby altering the degradation pathway and reducing the energy required for thermal decomposition.

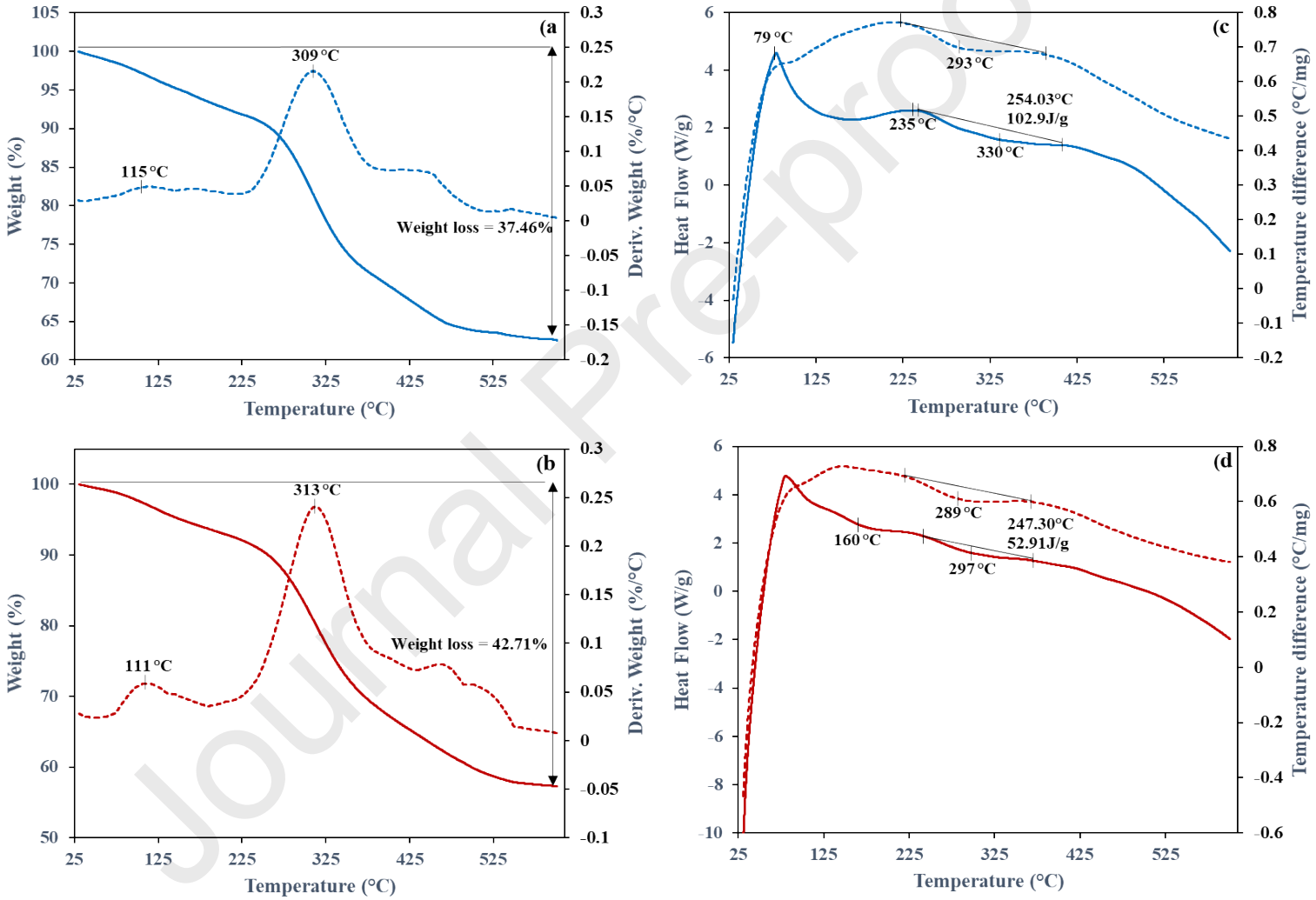

Figure 5. Thermal analysis of semi-IPN films. (a, b) TGA curves of CMC/SiO_2 and CMC/SiO_2/AgCl samples, respectively. (c, d) DSC thermograms of CMC/SiO_2 and CMC/SiO_2/AgCl samples, respectively.

3.3 Swelling behavior

To evaluate the pH-responsive behavior of the semi-IPN films, Selected CMC/SiO_2 and CMC/SiO_2/AgCl semi-IPN films were subjected to swelling analysis. Swelling tests were conducted in aqueous media at pH 3 and pH 10 during 24 hours. The selected pH values were chosen to represent two extreme conditions of the pH-responsive behavior of the semi-IPN films based on the pKa of CMC (approximately 4.3). At pH 3, which is below the pKa, the carboxylic groups are predominantly protonated (-COOH), resulting in reduced electrostatic repulsion and limited swelling. In contrast, at pH 10, which is well above the pKa, the carboxylic groups are largely deprotonated ($-COO^-$), leading to increased electrostatic repulsion and osmotic pressure, and consequently enhanced swelling.

As shown in Figure 6, the films exhibited pronounced swelling behavior at pH 10, whereas only limited swelling was observed at pH 3. Most of the swelling occurred within the first few hours, while only minor changes were observed between 6 h and 24 h, indicating that the films approached equilibrium swelling. The volume of the CMC/SiO_2 film increased by approximately 850.08 ± 34.04%. This high swelling ratio at pH 10 is attributed to the electrostatic repulsion between deprotonated carboxylate groups ($-COO^-$) within the semi-IPN network, which promotes expansion of the gel structure. In contrast, at acidic pH 3, only a slight volume increase was observed, likely due to physical water absorption on the film surface [65,66]. Under these acidic conditions, the films exhibited noticeable shrinkage relative to their swollen state at pH 10 because the environmental pH was below the pKa of the system, resulting in protonation of the carboxylate groups and reduced electrostatic repulsion. Although the films remained hydrated, swelling was significantly lower under acidic conditions because protonation of the carboxyl groups reduced electrostatic repulsion within the network. Incorporation of AgCl into the system led to a reduced swelling ratio in both basic and acidic conditions. The presence of silver compounds introduced subtle structural changes and

increased the compactness of the network, leading to lower permeability and reduced swelling capacity of the CMC/SiO_2/AgCl semi-IPN thin films.

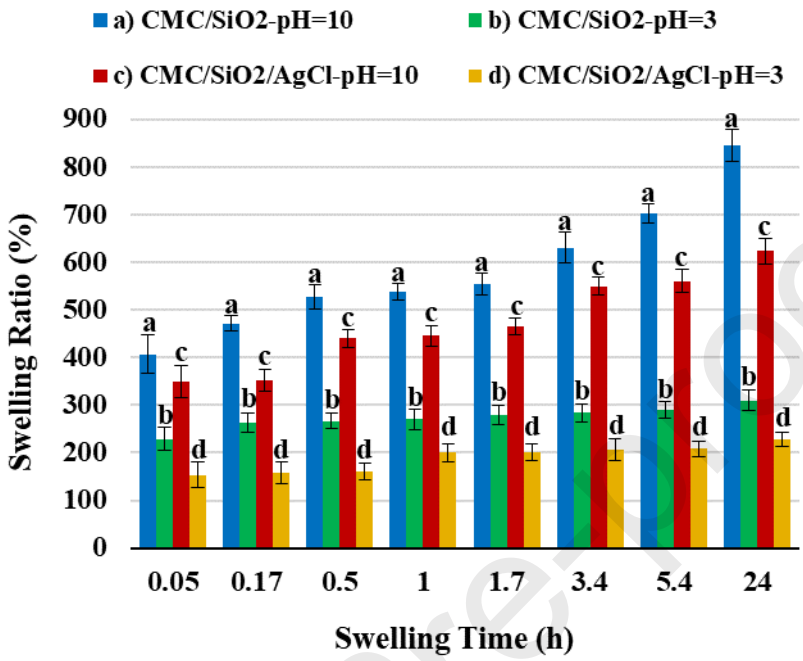

Figure 6. Swelling ratio of CMC/SiO_2 and CMC/SiO_2/AgCl semi-IPN films measured in aqueous media at pH 3 and pH 10. (mean ± SD, n=3)

To evaluate the response rate and reversibility of the swelling process, the CMC/SiO_2 sample was cyclically transferred between media of pH 10 and pH 3 at 5-minute intervals. The results, shown in Figure 7, demonstrate that following the initial swelling in the alkaline medium—resulting in a noticeable volume increase—the sample exhibited stable equilibrium and reversible swelling–shrinking behavior over the course of one hour. These reversible swelling–deswelling cycles demonstrate the excellent pH responsiveness of the semi-IPN films and support their potential applications in smart drug delivery systems, biosensors, and responsive membranes [67–69].

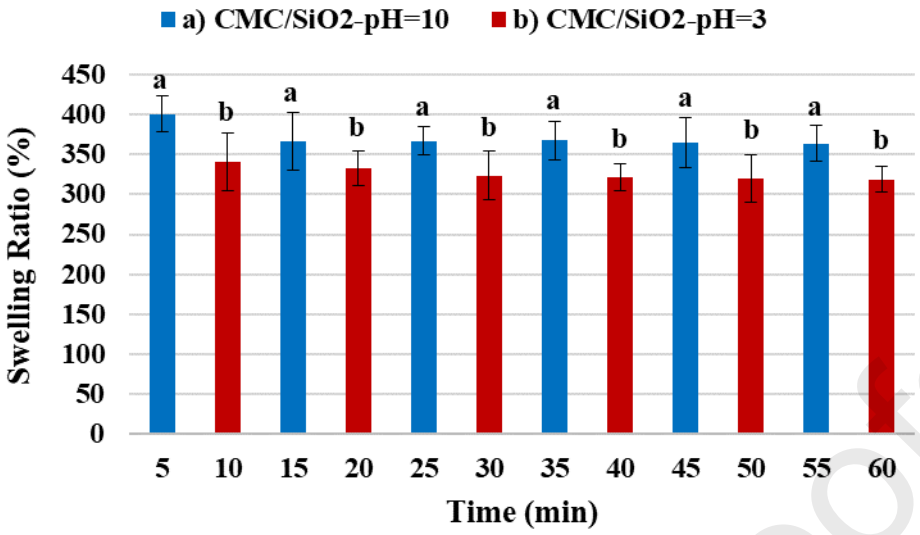

Figure 7. Effect of pH on the dynamic swelling behavior of the CMC/SiO_2 semi-IPN film (mean ± SD, n=3)

3.4 Antibacterial activity

The antibacterial activity of CMC/SiO_2 and CMC/SiO_2/AgCl semi-IPN films was evaluated against *Staphylococcus aureus* and *Escherichia coli*. Table 1 summarizes the antibacterial performance of the semi-IPN films. The CMC/SiO_2/AgCl film exhibited clear antibacterial activity against both bacterial strains, consistent with findings reported in previous studies on silver-containing compounds [33,70–72]. Moreover, no obvious difference in antibacterial activity was observed between the two bacterial strains, which is also in agreement with previous reports [70,73,74]. Although both samples showed an increase in the measured diameter after incubation (Fig. 8), part of this increase resulted from swelling of the hydrogel films on the moist agar surface. Therefore, the measured diameter represents the combined contribution of film swelling and the surrounding inhibition zone. This effect is more pronounced for the CMC/SiO_2 film, where the increase in the measured diameter was mainly associated with hydrogel swelling rather than antibacterial inhibition. In contrast, the CMC/SiO_2/AgCl film exhibited a distinct inhibition zone in addition to limited swelling,

confirming that the observed antibacterial activity originated from the incorporation of AgCl within the semi-IPN network.

Table 1. Zone of inhibition (mm) for CMC/SiO_2 and CMC/SiO_2/AgCl semi-IPN films against *Escherichia coli* and *Staphylococcus aureus*

Films	Sample Diameter	Measured inhibition diameter (mm)	
		Escherichia coli	*Streptococcus*
CMC/SiO_2	7.0	11.0	10.0
CMC/SiO_2/AgCl	7.0	9.5	9.5

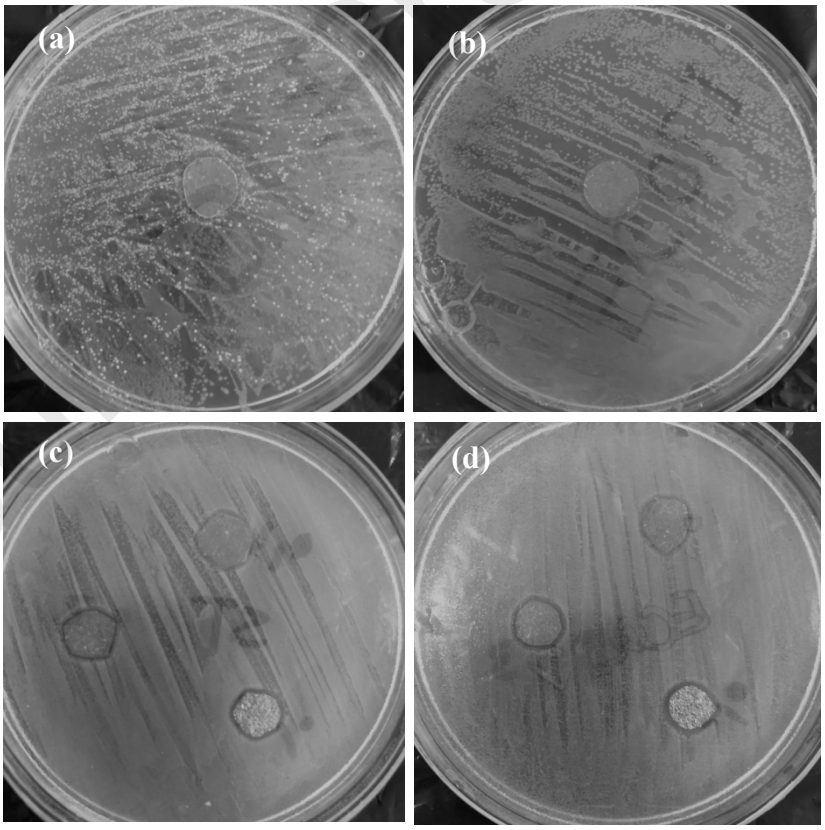

Figure 8. Zone of inhibition of semi-IPN films against Escherichia coli and Staphylococcus aureus. (a, b) CMC/SiO_2 film tested against *S. aureus* and *E. coli*, respectively. (c, d) CMC/SiO_2/AgCl film tested against *S. aureus* and *E. coli*, respectively.

3.4 In vitro cytocompatibility assessment by MTT assay

Figure 9 presents the in vitro cell viability of CMC/SiO_2 and CMC/SiO_2/AgCl semi-IPN films as determined by the MTT assay. According to ISO 10993-5 standards, none of the developed hybrid materials exhibited cytotoxicity, with cell viability values exceeding the acceptable threshold of 70% compared to control samples [75,76]. The CMC/SiO_2 sample demonstrated excellent cytocompatibility, indicating its potential suitability for biomedical applications. The favorable cytocompatibility observed in the CMC/SiO_2 semi-IPN suggests that this hybrid platform may be further functionalized for specific biomedical applications. The CMC/SiO_2/AgCl sample, designed as an antimicrobial coating, also maintained acceptable cytocompatibility while exhibiting antibacterial activity. Depending on the intended biomedical application, the AgCl content could be adjusted to optimize the balance between antibacterial activity and cytocompatibility [77,78].

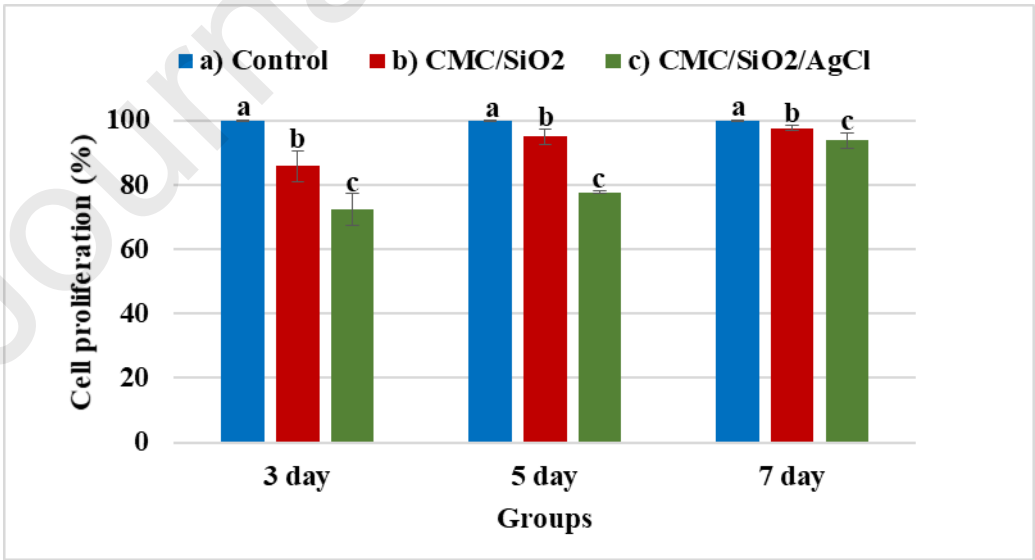

Figure 9. MTT assay results for CMC/SiO_2, CMC/SiO_2/AgCl, and control groups after 3, 5, and 7 days of incubation. (mean ± SD, n=3)

3.5 Comparison with recently reported smart hydrogel systems

Table 2 compares the characteristics of the present semi-IPN hydrogel films with representative smart hydrogel systems reported in recent literature. Recent studies have mainly focused on the development of multifunctional hydrogels with properties such as self-healing, conductivity, bioadhesion, and wearable sensing capabilities. In contrast, the CMC/SiO_2/AgCl semi-IPN films developed in this work combine pH-responsive swelling, antibacterial activity, cytocompatibility, and facile fabrication using low-cost and commercially available raw materials. These combined characteristics make the proposed system attractive for practical applications in drug delivery, wound healing, active packaging, and other smart biomedical applications.

Table 2. Comparison of recently reported smart hydrogels and the present work regarding responsive behavior, unique advantages, and potential applications.

Application	**Unique Advantage**	**Smart Functionality**	**Base Material**	**Reference**
• Wound healing • multi-signal skin monitoring • bioelectronics	• Rapid self-healing • Photothermal conversion • Injectability • Strain sensing	Self-healing and photothermal response	CMCS/Silk sericin/	Dang et al. (2025)[8]
• motion monitoring • human-computer interaction • wearable sensors	• Antimicrobial activity • Strong adhesion • Biocompatibility • Simple fabrication	Temperature- and pH-responsive	CMC/Dopamine	Dang et al.(2025)[5]
• soft robotics • flexible electronics • wearable devices	• High stretchability • Electrical conductivity • Antifreezing behaviour • Rapid self-healing	Self-healing and conductive response	CMCS/PVA /LiCl/Fe^{3+}	Yuntao et al. (2025)[9]

Application	Unique Advantage	Smart Functionality	Base Material	Reference
• **Drug delivery** • **wound dressing** • **Smart packaging** • **biosensing**	• **pH-responsive swelling** • **Antibacterial activity** • **Excellent cytocompatibility** • **Thin-film architecture** • **Low-cost fabrication**	**pH-responsive swelling**	**CMC/SiO_2/ AgCl**	**This work**

4. Conclusion

The incorporation of CMC into the SiO_2 framework through hydrogen-bond interactions led to the formation of thin semi-interpenetrating polymer network films (CMC/SiO_2 semi-IPN) with a thickness of approximately 0.3 mm. This modification improved the mechanical integrity and pH responsiveness, resulting in a maximum swelling ratio of 850 ± 34%. In addition, the incorporation of silver ions into the hybrid network provided antibacterial functionality, producing inhibition zones of 9.5 mm against both E. coli and B. subtilis, while only slightly compromising the swelling behavior of the hydrogel films.

The resulting flexible, pH-responsive semi-IPN hydrogel thin layer films incorporated TEOS-derived silica and antibacterial silver species, thereby enabling simultaneous structural reinforcement and functional responsiveness through a simple, eco-friendly manufacturing method. Structural and physicochemical analyses confirmed the successful formation of the semi-IPN structure, which improved material stability and practical performance. The hydrogel films displayed pronounced, reversible pH-responsive swelling, expanding in alkaline environments and contracting in acidic environments, thereby underscoring their potential for smart and stimuli-responsive applications.

Furthermore, the incorporation of silver-based active agents endowed the semi-IPN films with effective antibacterial activity against E. coli and B. subtilis (9.5 mm inhibition zones), while maintaining high cell viability (>93%), well above the ISO 10993-5 cytocompatibility

threshold. Although silver loading induced minor alterations in structural and physical properties, the overall pH-responsive swelling performance was maintained, demonstrating that the semi-IPN framework can effectively accommodate functional additives.

Ultimately, this work demonstrates that CMC/SiO_2-based semi-IPN hydrogel films combine pH-responsive swelling, antibacterial activity, cytocompatibility, and low-cost fabrication within a single multifunctional platform. The tunability of the system, achieved by substituting silver with alternative active agents, offers further opportunities for application-specific optimization. Future studies will focus on in vivo biocompatibility assessment and on the incorporation of alternative bioactive agents to further enhance the antimicrobial and functional performance of the semi-IPN films.

Acknowledgments

We gratefully acknowledge Mehrafarin Fesharaki for her leadership in the MTT assay analysis, Prof. Mohsen Nekoeinia for statistical analysis and guidance, and Dr. Amir Sadeghi for his critical review of the manuscript, valuable scientific comments, and careful language editing.

CRediT authorship contribution statement

Gelare Sadeghi Borojeni: Conceptualization, Methodology, Investigation, Formal analysis, Data curation, Visualization, Writing – original draft.

Majid Kolahdoozan: Conceptualization, Supervision, Resources, Project administration, Writing – review & editing.

Rokhsareh Meamar: Supervision, Scientific consultation.

References

[1] A. Olad, J. Aghayan, H. Gharekhani, M. Akbarzadeh, Carboxymethyl cellulose-based semi-IPN hydrogel nanocomposite with improved physicochemical and mechanical properties, J Polym Res 29 (2022) 460. https://doi.org/10.1007/s10965-022-03307-9.

[2] K. Koshenaj, G. Ferrari, A Comprehensive Review on Starch-Based Hydrogels: From Tradition to Innovation, Opportunities, and Drawbacks, Polymers 16 (2024) 1991. https://doi.org/10.3390/polym16141991.

[3] X. Dang, S. Han, J. Tang, X. Wang, Functional Starch-Based Conductive Hydrogel for Flexible Electronics: Design, Construction, and Applications, Aggregate 6 (2025) e70121. https://doi.org/10.1002/agt2.70121.

[4] Y. Gupta, M. Sohail Khan, M. Bansal, M. Kumar Singh, K. Pragatheesh, A. Thakur, A review of carboxymethyl cellulose composite-based hydrogels in drug delivery applications, Results in Chemistry 10 (2024) 101695. https://doi.org/10.1016/j.rechem.2024.101695.

[5] X. Dang, B. Guo, Y. Fu, Y. Fei, X. Wang, All-natural biomass-based multifunctional conductive hydrogel for an all-in-one wearable strain sensor, Cell Biomaterials 1 (2025). https://doi.org/10.1016/j.celbio.2025.100076.

[6] X. Dang, Y. Fu, X. Wang, Versatile Biomass-Based Injectable Photothermal Hydrogel for Integrated Regenerative Wound Healing and Skin Bioelectronics, Advanced Functional Materials 34 (2024) 2405745. https://doi.org/10.1002/adfm.202405745.

[7] F. Hong, P. Qiu, Y. Wang, P. Ren, J. Liu, J. Zhao, D. Gou, Chitosan-based hydrogels: From preparation to applications, a review, Food Chemistry: X 21 (2024) 101095. https://doi.org/10.1016/j.fochx.2023.101095.

[8] X. Dang, J. Tang, S. Han, X. Wang, M. Tao, M. Zheng, Injectable Self-Healing Biomass-Based Hydrogel Bioadhesive Integrating Skin Bioelectronics and Regenerative Wound Healing, Advanced Functional Materials 36 (2026) e30332. https://doi.org/10.1002/adfm.202530332.

[9] Y. Fu, X. Dang, Bio-Inspired Highly Stretchable and Ultrafast Autonomous Self-Healing Supramolecular Hydrogel for Multifunctional Durable Self-Powered Wearable Devices, Small 21 (2025) 2408640. https://doi.org/10.1002/smll.202408640.

[10] H. Wang, L. Yang, Y. Yang, A review of sodium alginate-based hydrogels: Structure, mechanisms, applications, and perspectives, International Journal of Biological Macromolecules 292 (2025) 139151. https://doi.org/10.1016/j.ijbiomac.2024.139151.

[11] R. Kundu, P. Mahada, B. Chhirang, B. Das, Cellulose hydrogels: Green and sustainable soft biomaterials, Current Research in Green and Sustainable Chemistry 5 (2022) 100252. https://doi.org/10.1016/j.crgsc.2021.100252.

[12] Y. Cao, L. Huang, J. Chen, J. Liang, S. Long, Y. Lu, Development of a controlled release formulation based on a starch matrix system, International Journal of Pharmaceutics 298 (2005) 108–116. https://doi.org/10.1016/j.ijpharm.2005.04.005.

[13] S. Bongiovanni Abel, C.A. Busatto, F. Karp, D. Estenoz, M. Calderón, Weaving the next generation of (bio)materials: Semi-interpenetrated and interpenetrated polymeric networks for biomedical applications, Advances in Colloid and Interface Science 321 (2023) 103026. https://doi.org/10.1016/j.cis.2023.103026.

[14] M. Mumtaz, N. Hussain, M. Ashraf, H.M.H. Azam, A. Iftikhar, Introduction to Biopolymers, Their Blend, IPN s, Gel, Composites, and Nanocomposites, in: Applications of Biopolymers in Science, Biotechnology, and Engineering, John Wiley & Sons, Ltd, 2024: pp. 1–29. https://doi.org/10.1002/9781119783473.ch1.

[15] C. Cona, K. Bailey, E. Barker, Characterization Methods to Determine Interpenetrating Polymer Network (IPN) in Hydrogels, Polymers 16 (2024) 2050. https://doi.org/10.3390/polym16142050.

[16] N. Zoratto, P. Matricardi, 4 - Semi-IPNs and IPN-based hydrogels, in: K. Pal, I. Banerjee (Eds.), Polymeric Gels, Woodhead Publishing, 2018: pp. 91–124. https://doi.org/10.1016/B978-0-08-102179-8.00004-1.

[17] T.M. Aminabhavi, M.N. Nadagouda, U.A. More, S.D. Joshi, V.H. Kulkarni, M.N. Noolvi, P.V. Kulkarni, Controlled release of therapeutics using interpenetrating polymeric networks, Expert Opinion on Drug Delivery 12 (2015) 669–688. https://doi.org/10.1517/17425247.2014.974871.

[18] H. Chen, C. Regeard, H. Salmi, F. Morlet-Savary, N. Giacoletto, M. Nechab, P. Xiao, F. Dumur, J. Lalevée, Interpenetrating polymer network hydrogels using natural based dyes initiating systems: Antibacterial activity and 3D/4D performance, European Polymer Journal 166 (2022) 111042. https://doi.org/10.1016/j.eurpolymj.2022.111042.

[19] M. Bustamante-Torres, D. Romero-Fierro, B. Arcentales-Vera, K. Palomino, H. Magaña, E. Bucio, Hydrogels Classification According to the Physical or Chemical Interactions and as Stimuli-Sensitive Materials, Gels 7 (2021) 182. https://doi.org/10.3390/gels7040182.

[20] S. Erkeçoğlu, A.D. Sezer, S. Bucak, Smart Delivery Systems with Shape Memory and Self-Folding Polymers, in: A.D. Sezer (Ed.), Smart Drug Delivery System, IntechOpen, Rijeka, 2016. https://doi.org/10.5772/62199.

[21] Z. Ahmad, S. Salman, S.A. Khan, A. Amin, Z.U. Rahman, Y.O. Al-Ghamdi, K. Akhtar, E.M. Bakhsh, S.B. Khan, Versatility of Hydrogels: From Synthetic Strategies, Classification, and Properties to Biomedical Applications, Gels 8 (2022) 167. https://doi.org/10.3390/gels8030167.

[22] N. Asadi, A.R. Del Bakhshayesh, S. Davaran, A. Akbarzadeh, Common biocompatible polymeric materials for tissue engineering and regenerative medicine, Materials Chemistry and Physics 242 (2020) 122528. https://doi.org/10.1016/j.matchemphys.2019.122528.

[23] J. Mazuryk, P.S. Sharma, W. Kutner, Chapter 8 - Molecularly imprinted polymer composites in drug delivery, in: M.P. Sooraj, A.S. Nair, B. Mathew, S. Thomas (Eds.), Molecularly Imprinted Polymer Composites, Woodhead Publishing, 2021: pp. 173–226. https://doi.org/10.1016/B978-0-12-819952-7.00014-7.

[24] S. Dutta, R. Sen Gupta, S. Pathan, S. Bose, Interpenetrating polymer networks for desalination and water remediation: a comprehensive review of research trends and prospects, RSC Advances 13 (2023) 6087–6107. https://doi.org/10.1039/D2RA07843K.

[25] E.D. Barker, Preclinical Evaluation of a Novel Polysaccharide Hydrogel for Local Chemotherapy Delivery to Solid Tumors, The University of Tennessee Health Science Center, 2014.

[26] A.K. Nayak, M.S. Hasnain, T.M. Aminabhavi, Drug delivery using interpenetrating polymeric networks of natural polymers: A recent update, Journal of Drug Delivery Science and Technology 66 (2021) 102915.

[27] R. Censi, C. Casadidio, S. Deng, M.R. Gigliobianco, M.G. Sabbieti, D. Agas, F. Laus, P. Di Martino, Interpenetrating hydrogel networks enhance mechanical stability, rheological properties, release behavior and adhesiveness of platelet-rich plasma, International Journal of Molecular Sciences 21 (2020) 1399.

[28] M. Upadhyay, S.K.R. Adena, H. Vardhan, S.K. Yadav, B. Mishra, Development of biopolymers based interpenetrating polymeric network of capecitabine: a drug delivery vehicle to extend the release of the model drug, International Journal of Biological Macromolecules 115 (2018) 907–919.

[29] S. Xu, H. Li, H. Ding, Z. Fan, P. Pi, J. Cheng, X. Wen, Allylated chitosan-poly (N-isopropylacrylamide) hydrogel based on a functionalized double network for controlled drug release, Carbohydrate Polymers 214 (2019) 8–14.

[30] Z. Shi, X. Gao, M.W. Ullah, S. Li, Q. Wang, G. Yang, Electroconductive natural polymer-based hydrogels, Biomaterials 111 (2016) 40–54. https://doi.org/10.1016/j.biomaterials.2016.09.020.

[31] X. Tong, W. Pan, T. Su, M. Zhang, W. Dong, X. Qi, Recent advances in natural polymer-based drug delivery systems, Reactive and Functional Polymers 148 (2020) 104501. https://doi.org/10.1016/j.reactfunctpolym.2020.104501.

[32] S. Sagar, A. Alturki, M. Farhan, A. Bahadar, N. Hossain, Synergistic influence of tetraethyl orthosilicate crosslinker on mixed matrix hydrogels, Appl Nanosci 12 (2022) 2923–2932. https://doi.org/10.1007/s13204-022-02606-3.

[33] H.E. Emam, A.P. Manian, B. Široká, H. Duelli, B. Redl, A. Pipal, T. Bechtold, Treatments to impart antimicrobial activity to clothing and household cellulosic-textiles – why "*Nano*"-silver?, Journal of Cleaner Production 39 (2013) 17–23. https://doi.org/10.1016/j.jclepro.2012.08.038.

[34] S.-B. Park, J.-O. You, H.-Y. Park, S.J. Haam, W.-S. Kim, A Novel pH-Sensitive Membrane from Chitosan — TEOS IPN; Preparation and Its Drug Permeation Characteristics, Biomaterials 22 (2001) 323–330. https://doi.org/10.1016/S0142-9612(00)00187-3.

[35] W.L. Huang, K. Ming Liang, S. Ren Gu, Effect of HCl in a two-step sol–gel process using TEOS, Journal of Non-Crystalline Solids 258 (1999) 234–238. https://doi.org/10.1016/S0022-3093(99)00551-7.

[36] D.A. Donatti, D.R. Vollet, Effects of HCl on the ultrasound catalyzed TEOS hydrolysis as determined by a calorimetric study, Journal of Non-Crystalline Solids 208 (1996) 99–104. https://doi.org/10.1016/S0022-3093(96)00508-X.

[37] A.H. Boonstra, T.N.M. Bernards, Hydrolysis-condensation reactions in the acid step of a two-step silica sol-gel process, investigated with 29Si NMR at −75°C, Journal of Non-Crystalline Solids 108 (1989) 249–259. https://doi.org/10.1016/0022-3093(89)90295-0.

[38] Y. Sato, A. Sugimoto, T. Iwashina, R. Hayami, K. Yamamoto, T. Gunji, Hydrolysis and condensation behavior of tetraethoxysilane, hexaethoxydisiloxane, and octaethoxytrisiloxane, J Sol-Gel Sci Technol 108 (2023) 377–391. https://doi.org/10.1007/s10971-023-06159-x.

[39] B.A. Serban, E. Barrett-Catton, M.A. Serban, Tetraethyl Orthosilicate-Based Hydrogels for Drug Delivery—Effects of Their Nanoparticulate Structure on Release Properties, Gels 6 (2020) 38. https://doi.org/10.3390/gels6040038.

[40] A.C. Hernández-González, L. Téllez-Jurado, L.M. Rodríguez-Lorenzob, SYNTHESIS OF IN-SITU SILICA-ALGINATE HYBRID HYDROGELS BY A SOL-GEL ROUTE, Carbohydrate Polymers 250 (2020) 116877. https://doi.org/10.1016/j.carbpol.2020.116877.

[41] S.N. Jayash, P.R. Cooper, R.M. Shelton, S.A. Kuehne, G. Poologasundarampillai, Novel Chitosan-Silica Hybrid Hydrogels for Cell Encapsulation and Drug Delivery, International Journal of Molecular Sciences 22 (2021) 12267. https://doi.org/10.3390/ijms222212267.

[42] J. Liu, C. Zhang, D. Miao, S. Sui, F. Deng, C. Dong, L. Zhang, P. Zhu, Preparation and Characterization of CarboxymethylCellulose Hydrogel Fibers, Journal of Engineered Fibers and Fabrics 13 (2018) 155892501801300302. https://doi.org/10.1177/155892501801300302.

[43] R.R. Mohamed, M.E. Fahim, S.M.A. Soliman, Development of hydrogel based on Carboxymethyl cellulose/poly(4-vinylpyridine) for controlled releasing of fertilizers, BMC Chemistry 16 (2022) 52. https://doi.org/10.1186/s13065-022-00846-6.

[44] R. Badry, M.M. El-Nahass, N. Nada, H. Elhaes, M.A. Ibrahim, Structural and UV-blocking properties of carboxymethyl cellulose sodium/CuO nanocomposite films, Sci Rep 13 (2023) 1123. https://doi.org/10.1038/s41598-023-28032-1.

[45] M. Youshi, M.R. Farahpour, Z.G. Tabatabaei, Facile fabrication of carboxymethylcellulose/ZnO/g-C3N4 containing nutmeg extract with photocatalytic performance for infected wound healing, Sci Rep 13 (2023) 18704. https://doi.org/10.1038/s41598-023-45921-7.

[46] S. Ali, M. Mansha, N. Baig, S.A. Khan, Cost-Effective and Selective Fluorescent Chemosensor (Pyr-NH@SiO2 NPs) for Mercury Detection in Seawater, Nanomaterials 12 (2022) 1249. https://doi.org/10.3390/nano12081249.

[47] A.M.A. Coco, T. Martins, B.R. Barrioni, M. de M. Pereira, Effect of incorporating silver on the structure and ion release profile of binary SiO2–Ag2O mesoporous bioactive glass submicron spherical particles, Ceramics International 47 (2021) 26100–26108. https://doi.org/10.1016/j.ceramint.2021.06.016.

[48] J.-X. Wang, L.-X. Wen, Z.-H. Wang, J.-F. Chen, Immobilization of silver on hollow silica nanospheres and nanotubes and their antibacterial effects, Materials Chemistry and Physics 96 (2006) 90–97. https://doi.org/10.1016/j.matchemphys.2005.06.045.

[49] B. Vinoda, M. Vinuth, Photocatalytic degradation of toxic methyl red dye using silica nanoparticles synthesized from rice husk ash, Journal of Environmental & Analytical Toxicology 5 (2022).

[50] S. Du, X. Chen, X. Chen, S. Li, G. Yuan, T. Zhou, J. Li, Y. Jia, D. Xiong, H. Tan, Covalent chitosan-cellulose hydrogels via schiff-base reaction containing macromolecular microgels for pH-sensitive drug delivery and wound dressing, Macromolecular Chemistry and Physics 220 (2019) 1900399.

[51] S.M. Alshehri, A. Aldalbahi, A.B. Al-hajji, A.A. Chaudhary, M. in het Panhuis, N. Alhokbany, T. Ahamad, Development of carboxymethyl cellulose-based hydrogel and nanosilver composite as antimicrobial agents for UTI pathogens, Carbohydrate Polymers 138 (2016) 229–236. https://doi.org/10.1016/j.carbpol.2015.11.004.

[52] N.S.V. Capanema, I.C. Carvalho, A.A.P. Mansur, S.M. Carvalho, A.P. Lage, H.S. Mansur, Hybrid Hydrogel Composed of Carboxymethylcellulose–Silver Nanoparticles–Doxorubicin for Anticancer and Antibacterial Therapies against Melanoma Skin Cancer Cells, ACS Appl. Nano Mater. 2 (2019) 7393–7408. https://doi.org/10.1021/acsanm.9b01924.

[53] A.M. Adel, H. Abou-Youssef, A.A. El-Gendy, A.M. Nada, Carboxymethylated Cellulose Hydrogel; Sorption Behavior and Characterization, (n.d.).

[54] S.D. Yuwono, E. Wahyuningsih, Noviany, A.A. Kiswandono, W. Simanjuntak, S. Hadi, Characterization of Carboxymethyl Cellulose (CMC) Synthesized from Microcellulose of Cassava Peel, Mater. Plast. 57 (2021) 225–235. https://doi.org/10.37358/mp.20.4.5422.

[55] C.-C. Yang, Y.J. Li, T.-H. Liou, Preparation of novel poly(vinyl alcohol)/SiO2 nanocomposite membranes by a sol–gel process and their application on alkaline DMFCs, Desalination 276 (2011) 366–372. https://doi.org/10.1016/j.desal.2011.03.079.

[56] Z. Jamalpoor, H. Ahmadi, M. Abdous, A. Rahdar, CMC/Starch/SiO2/ GQDs nanoemulsion for targeted delivery of 5-fluorouracil, Journal of Molecular Liquids 408 (2024) 125407. https://doi.org/10.1016/j.molliq.2024.125407.

[57] T.S. Soliman, Effects of SiO2 Nanoparticles on Polyvinyl Alcohol/Carboxymethyl Cellulose Polymer Blend Films' Structural, Wettability, Surface Roughness, and Optical Characteristics, Advances in Polymer Technology 2024 (2024) 3623198. https://doi.org/10.1155/2024/3623198.

[58] H. Hassan Afandy, D.K. Sabir, S.B. Aziz, Antibacterial Activity of the Green Synthesized Plasmonic Silver Nanoparticles with Crystalline Structure against Gram-Positive and Gram-Negative Bacteria, Nanomaterials 13 (2023) 1327. https://doi.org/10.3390/nano13081327.

[59] J.-K. Yan, P.-F. Cai, X.-Q. Cao, H.-L. Ma, Q. Zhang, N.-Z. Hu, Y.-Z. Zhao, Green synthesis of silver nanoparticles using 4-acetamido-TEMPO-oxidized curdlan, Carbohydrate Polymers 97 (2013) 391–397. https://doi.org/10.1016/j.carbpol.2013.05.049.

[60] M.S.A. Rani, S. Rudhziah, A. Ahmad, N.S. Mohamed, Biopolymer Electrolyte Based on Derivatives of Cellulose from Kenaf Bast Fiber, Polymers 6 (2014) 2371–2385. https://doi.org/10.3390/polym6092371.

[61] Cellulose and Paper Department, National Research Centre, 33, El Bohouth Str., P.O. 12622, Dokki Giza, Egypt, M. El-Sakhawy, H.-A.S. Tohamy, Cellulose and Paper Department, National Research Centre, 33, El Bohouth Str., P.O. 12622, Dokki Giza, Egypt, A. Salama, Cellulose and Paper Department, National Research Centre, 33, El Bohouth Str., P.O. 12622, Dokki Giza, Egypt, S. Kamel, Cellulose and Paper Department, National Research Centre, 33, El Bohouth Str., P.O. 12622, Dokki Giza, Egypt, THERMAL PROPERTIES OF CARBOXYMETHYL CELLULOSE ACETATE BUTYRATE, Cellulose Chem. Technol. 53 (2019) 667–675. https://doi.org/10.35812/CelluloseChemTechnol.2019.53.65.

[62] Y. Shin, D. Kim, Y. Hu, Y. Kim, I.K. Hong, M.S. Kim, S. Jung, pH-Responsive Succinoglycan-Carboxymethyl Cellulose Hydrogels with Highly Improved Mechanical Strength for Controlled Drug Delivery Systems, Polymers 13 (2021) 3197. https://doi.org/10.3390/polym13183197.

[63] N.S.V. Capanema, A.A.P. Mansur, A.C. de Jesus, S.M. Carvalho, L.C. de Oliveira, H.S. Mansur, Superabsorbent crosslinked carboxymethyl cellulose-PEG hydrogels for potential wound dressing applications, International Journal of Biological Macromolecules 106 (2018) 1218–1234. https://doi.org/10.1016/j.ijbiomac.2017.08.124.

[64] A.M. Salem, A.R. Mohamed, A.Y. Yassin, The Effect of Low Concentrations of Polypyrrole on the Structural, Thermal, and Dielectric Characteristics of CMC/PPy Blends, J Mater Sci: Mater Electron 34 (2023) 1522. https://doi.org/10.1007/s10854-023-10938-1.

[65] C. Chang, M. He, J. Zhou, L. Zhang, Swelling Behaviors of pH- and Salt-Responsive Cellulose-Based Hydrogels, Macromolecules 44 (2011) 1642–1648. https://doi.org/10.1021/ma102801f.

[66] N.F.C. Nan, N. Zainuddin, M. Ahmad, Preparation and Swelling Study of CMC Hydrogel as Potential Superabsorbent, (2019).

[67] A. Das, A. Kumar, N.B. Patil, C. Viswanathan, D. Ghosh, Preparation and characterization of silver nanoparticle loaded amorphous hydrogel of carboxymethylcellulose for infected wounds, Carbohydrate Polymers 130 (2015) 254–261. https://doi.org/10.1016/j.carbpol.2015.03.082.

[68] S. Dutta, P. Samanta, D. Dhara, Temperature, pH and redox responsive cellulose based hydrogels for protein delivery, International Journal of Biological Macromolecules 87 (2016) 92–100. https://doi.org/10.1016/j.ijbiomac.2016.02.042.

[69] J. Tan, R. Liu, W. Wang, W. Liu, Y. Tian, M. Wu, Y. Huang, Controllable Aggregation and Reversible pH Sensitivity of AuNPs Regulated by Carboxymethyl Cellulose, Langmuir 26 (2010) 2093–2098. https://doi.org/10.1021/la902593e.

[70] T. Angelova, N. Rangelova, H. Dineva, N. Georgieva, R. Müller, Synthesis, characterization and antibacterial assessment of SiO2-hydroxypropylmethyl cellulose hybrid materials with embedded silver nanoparticles, Biotechnol Biotechnol Equip 28 (2014) 747–752. https://doi.org/10.1080/13102818.2014.944789.

[71] S. Kaviya, J. Santhanalakshmi, B. Viswanathan, J. Muthumary, K. Srinivasan, Biosynthesis of silver nanoparticles using citrus sinensis peel extract and its antibacterial activity, Spectrochimica Acta Part A: Molecular and Biomolecular Spectroscopy 79 (2011) 594–598. https://doi.org/10.1016/j.saa.2011.03.040.

[72] N. Khandan Nasab, Z. Sabouri, S. Ghazal, M. Darroudi, Green-based synthesis of mixed-phase silver nanoparticles as an effective photocatalyst and investigation of their antibacterial properties, Journal of Molecular Structure 1203 (2020) 127411. https://doi.org/10.1016/j.molstruc.2019.127411.

[73] J. Yu, L. Wang, Y. Zhao, C. Zhou, Preparation, characterization, and antibacterial property of carboxymethyl cellulose derivatives bearing tetrabutylammonium salt, International Journal of Biological Macromolecules 176 (2021) 72–77. https://doi.org/10.1016/j.ijbiomac.2021.02.063.

[74] M. Radmehr, A. Poursattar Marjani, A. Akhavan, Synthesis and characterization of antibacterial CMC/AAc/ZnO nanocomposite superabsorbent using gamma radiation, Sci Rep 15 (2025) 9345. https://doi.org/10.1038/s41598-025-93884-8.

[75] N.S.V. Capanema, A.A.P. Mansur, S.M. Carvalho, T. Martins, M.S. Gonçalves, R.S. Andrade, E.M.S. Dorneles, L.C.D. Lima, É.L.F.C. de Alvarenga, E.V.B. da Fonseca, M.A. de Sá, A.P. Lage, Z.I.P. Lobato, H.S. Mansur, Nanosilver-Functionalized Hybrid Hydrogels of Carboxymethyl Cellulose/Poly(Vinyl Alcohol) with Antibacterial Activity for Prevention and Therapy of Infections of Diabetic Chronic Wounds, Polymers 15 (2023) 4542. https://doi.org/10.3390/polym15234542.

[76] ISO 10993-5:2009 - Biological evaluation of medical devices — Part 5: Tests for in vitro cytotoxicity, (n.d.). https://www.iso.org/standard/36406.html (accessed July 31, 2025).

[77] N.S.V. Capanema, A.A.P. Mansur, S.M. Carvalho, L.L. Mansur, C.P. Ramos, A.P. Lage, H.S. Mansur, Physicochemical properties and antimicrobial activity of biocompatible carboxymethylcellulose-silver nanoparticle hybrids for wound dressing and epidermal repair, Journal of Applied Polymer Science 135 (2018) 45812. https://doi.org/10.1002/app.45812.

[78] C. Liao, Y. Li, S.C. Tjong, Bactericidal and Cytotoxic Properties of Silver Nanoparticles, International Journal of Molecular Sciences 20 (2019) 449. https://doi.org/10.3390/ijms20020449.

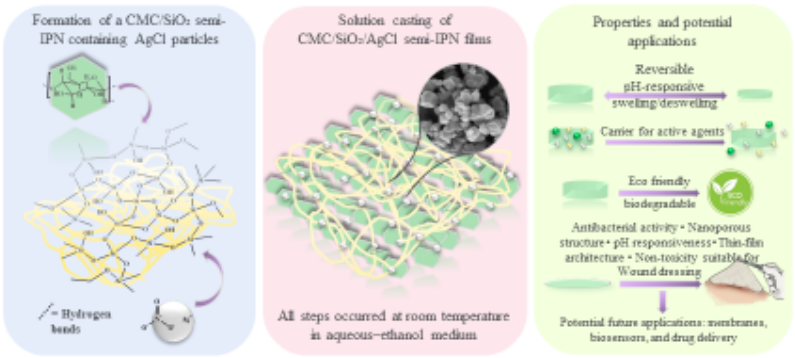

- Thin semi-interpenetrating polymer network hydrogel films exhibited reversible pH-responsive swelling of up to 850 ± 34%.
- Silver chloride incorporation imparted antibacterial activity against both Gram-negative and Gram-positive bacteria.
- The developed films combined pH-responsive behavior with excellent cytocompatibility (>93% cell viability).
- A simple, low-cost, and scalable fabrication strategy enabled the production of multifunctional hydrogel films.